INSTITUTE OF PHYSICS PUBLISHING JOURNAL OF PHYSICS D: APPLIED PHYSICS
J. Phys. D: Appl. Phys. **36** (2003) A49–A54 PII: S0022-3727(03)60117-8

Full three-dimensional modelling of curvature-dependent snow metamorphism: first results and comparison with experimental tomographic data

Frédéric Flin, Jean-Bruno Brzoska[1], Bernard Lesaffre, Cécile Coléou and Romeu André Pieritz

Météo-France, Centre d'Etudes de la Neige, 1441 r. de la Piscine, 38406 St Martin d'Hères Cedex, France

E-mail: jean-bruno.brzoska@meteo.fr

Received 14 September 2002
Published 22 April 2003
Online at stacks.iop.org/JPhysD/36/A49

Abstract
Snow, from its fall until its full melting, undergoes a structure metamorphism governed by temperature and humidity fields. Among the many possible mechanisms that contribute to snow metamorphism, those that depend only on curvature are the most accessible to modelling. The isothermal metamorphism of a dry snow sample near 0°C is addressed in this paper. Near 0°C, the vapour pressure of water is high: the metamorphism can be considered, in first approximation, as fully curvature-driven. This corresponds to neglect crystallographic orientation and diffusion-limited effects.

Based on Kelvin's and Langmuir–Knudsen equations, a growth law of the ice phase can be analytically obtained. In this law, the variation of the local volume fraction is proportional to the difference between integral and local curvatures. A simple numerical model was implemented in three dimensions and applied on real tomographic images.

1. Introduction

Dry natural snow ($T < 0$°C) can be considered as a volatile porous medium, prone to sublimation/condensation processes that alter its microstructure. Such metamorphism occurs in the presence of a temperature gradient (this often leads to faceted structures like depth hoar [1]), or not (then smooth shapes are obtained). In isothermal metamorphism, snow grains are allowed to evolve toward their equilibrium crystal shapes that minimize the surface energy of the set {grains + grain boundaries}. Close to 0°C, the vapour pressure is high and one can assume that possible grain boundary effects [2–4] would only affect the contact angle between grains. The rest of the grain surface is expected to be driven by the minimization of its local mean curvature, and possibly limited by vapour diffusion across the pores. The easiest way to carry out modelling is to take the local curvature as the only driving force. The validity of this assumption will be discussed in the following, and evaluated in a later work by running the model at a higher resolution ($>600^3$ voxels). We consider this stage as a starting point for modelling the metamorphism of real three-dimensional snow microstructures. We present a simple three-dimensional model based on the two-dimensional work of Bullard [5, 6], but using a more accurate geometric description of the grain surfaces [7–9]. It computes iteratively the curvature map of the three-dimensional snow image, then transfers solid matter from high to low mean curvature

[1] Author to whom correspondence should be addressed.

regions. Together with this model, we describe a recent experiment of isothermal metamorphism that is documented with tomographic images taken at the ESRF ID19 beamline. Although the image processing is still in progress, some preliminary tests of our model on subsamples of real data are finally presented and discussed.

2. Model

2.1. Principle

Here are presented the main hypotheses of our model and their physical motivations.

2.1.1. Driving force of the isothermal metamorphism. Isothermal metamorphism of a dry snow sample is known to be driven by the minimization of its interfacial energy. This results in a minimization of the difference in vapour partial pressure between two points of the ice surface. Let γ be the surface tension between ice and vapour and Ω the molar volume of ice. The vapour partial pressure $P(C)$ of a point of mean curvature C is given by the Kelvin's equation:

$$P(C) = P_0 \exp\left(\frac{2\gamma\Omega C}{RT}\right) \tag{1}$$

where R is the universal gas constant, T the temperature of snow and P_0 the vapour pressure on a flat surface. As generally $(2\gamma\Omega C/RT) \ll 1$, we have:

$$\Delta P = P - P_0 \simeq P_0\left(\frac{2\gamma\Omega C}{RT}\right) \tag{2}$$

2.1.2. Evaporation–condensation mechanism. Many mechanisms can be invoked to descript the mass transfer [10]. Intensive experimental work [11, 12] used laws from metallurgy [13] to find out the governing mechanisms. For experimental [14] and theoretical reasons [15], these works led to contradictory results. In our model, we assume that metamorphism is limited by the evaporation–condensation mechanism. This approximation corresponds to suppose that the vapour diffusion in the air is fast enough so that the vapour partial pressure is homogenous in the air phase. Surface diffusion, which generally occurs at first stages of the metamorphism [16] is neglected here. Due to its very high constant time, solid migration in the bulk is neglected too. Note that although ice matrix is a polycrystal, crystallographic orientations and grain boundary effects can generally be omitted for isothermal metamorphism at 'high' temperature (0 to -5°C). The evaporation–condensation is easy to implement and seems to be the mostly relevant to isothermal metamorphism: further validations of the model would confirm (or infirm) this mechanism. Assuming that Langmuir's equation is valid for mass transport in the gas phase, the flow rate, j, of the vapour deposition on a point of the surface is given by

$$j = \frac{\alpha(P_{\text{amb}} - P)}{(2\pi MRT)^{1/2}} \tag{3}$$

where P_{amb} is the ambient partial vapour pressure, α a positive constant and M the molar mass of water.

From equations (2) and (3), we have:

$$j = \alpha\gamma P_0\Omega\left(\frac{2}{\pi M(RT)^3}\right)^{1/2}(C_{\text{amb}} - C) \tag{4}$$

where C_{amb} denotes the curvature corresponding to the ambient partial vapour pressure.

Hence,

$$j = k(C_{\text{amb}} - C) \tag{5}$$

with k the rate constant of the evaporation–condensation mechanism. It can be noted that this formulation is equivalent to the surface-attachement-limited-kinetics (SALK) formulation introduced by Carter *et al* (see [6, 17]).

The change in solid volume fraction v_p of any surface volume element p during a time increment Δt can be expressed as:

$$\Delta v_p = j\frac{\Omega}{V_p^0}S_p\Delta t \tag{6}$$

where V_p^0 is the volume occupied by one volume element (voxel) and S_p the amount of surface lying within the voxel p.

Hence, we have

$$\Delta v_p = k_0(C_{\text{amb}} - C_p)S_p\Delta t \tag{7}$$

where k_0 is a constant term, independant of p.

To simulate a metamorphism where mass remains constant, C_{amb} should verify

$$C_{\text{amb}} = \frac{\sum_{\mathcal{S}} C_p S_p}{\sum_{\mathcal{S}} S_p} \tag{8}$$

where the voxels belonging to $\mathcal{S}$ are the surface voxels of the image.

Note that another expression of C_{amb} can be chosen to act as a source or a sink of matter. It can then simulate other evaporation–condensation mechanisms with global mass variation.

2.2. Algorithm

To each surface voxel is assigned a volume fraction value v_p, from -1 to 1, which accounts for the state of the surface boundary at a subvoxel scale: if the volume fraction is nearing -1, the considered voxel is about to disapear. If it is near 1, a neighbouring voxel will soon appear. When the levels of ± 1 are reached, the binary image is updated by adding or removing the appropriate voxels. The volume fractions v_p of the new interface voxels are then set to zero. At the beginning of the simulation, the volume fraction is assigned to zero for each surface voxel.

The algorithm consists in the following iterative method:

- The normal vector field of the binary image is first computed using an original discrete algorithm [8]. This adaptive method optimizes the smoothing of discretization effects while preserving relevant details of the numerical object.

- Then a three-dimensional curvature algorithm [7] is applied on this normal field: in each surface voxel p, the values $C_{1,p}$ and $C_{2,p}$ of the two-dimensional curvature are computed on two orthogonal planes by fitting the discrete arcs by a parabola. The three-dimensional curvature C_p on p is obtained as follows:

$$C_p = \tfrac{1}{2}(C_{1,p} + C_{2,p}) \tag{9}$$

- The curvature C_{amb} corresponding to the ambient vapour pressure is estimated according to equation (8). The quantity S_p, which depends on the normal vector in voxel p, is estimated by a voxel projection algorithm [9].
- For each surface voxel, the volume fraction variation Δv_p, which should be added to the previous value of v_p, is estimated according to equation (10). To save computation time, the time increment Δt is adapted at each stage of the metamorphism so that:

$$\Delta t = \frac{|\Delta v_p^{\max}|}{k_0 \max_{p\in\mathcal{S}}((|C_{\text{amb}} - C_p|)S_p)} \tag{10}$$

  where $\Delta v_p^{\max}$ is the volume fraction increment that corresponds to add or remove an entire voxel in one iteration, i.e. ± 1. As k_0 depends on numerous physical constants whose a part (in particular, α coefficient) is not precisely known, its value was arbitrary set to the unity. It implies that experimental and numerical times differ by an undetermined multiplicative constant.
- The new binary image is created according to the values of v_p:
  — if $v_p \leqslant -1$, the voxel p is removed of the ice phase.
  — if $v_p \geqslant +1$, p is removed of the vapour phase.
- The previous method is applied to the new image.

3. Experiment of isothermal metamorphism

3.1. X-ray microtomography

A three-month long experiment of isothermal metamorphism at -2°C was run at Col de Porte, Charteuse mountain, French Alps, to provide tomographic three-dimensional data for the validation of metamorphism models. Three-dimensional images of snow samples ($9 \times 9\,\text{mm}^2$ cylinders) were obtained at the ESRF ID19 beamline by x-ray absorption microtomography [18] using a specially designed refrigerated cell [19]. All the images were obtained at 18–20 keV, with a voxel size of 4.91 μm.

3.2. Sample preparation

A 0.5×1 m slab of recent snow was first collected on the field (on 01/16/02) 15 h after the snow fall (exterior temperature -1°C, slab thickness 12 cm), then stored in a closed styrodur box (to prevent sublimation) inside the cold room carefully held at $-2\pm0.2^{\circ}$C for three months; till the end of sampling, all manipulations were done in the cold room at this temperature. A 3 cm wide core was sampled at increasing intervals, ranging from 24 h at the beginning to one week at the end of the experiment. All samples were taken at mid-height of the slab, always more than 10 cm away from already sampled regions of the slab.

Once sampled, each core was impregnated by 1-chloronaphtalene (90% purity, ACROS, practical melting range after raw fractioned crystallization $-15/-20^{\circ}$C), then allowed to freeze and stored in a refrigerator at -20°C. Owing to the stiffness of its cyclic molecule, this low toxicity filler is readily machined close to its melting point; moreover, its absorption properties allow to distinguish ice, filler and remaining air bubbles on 9 mm wide samples at 18–20 keV. Of course, it does not dissolve water. At the end of the metamorphism experiments, the cold room was set to -25°C, each strengthened core was machined into the shape of a $9 \times 9\,\text{mm}^2$ cylinder and sealed into a gas-tight sample holder made of 0.2 mm thick plexiglas. Secured samples were stored till the beginning of the tomography in a refrigerator at -50°C.

3.3. Image processing

The grey-level images, reconstructed at the ESRF from each set of 1500 radiographs, were contoured using the following semi-automatic procedure:

- Normalization, then first neighbours three-dimensional averaging, i.e. three-dimensional averaging in a 3^3 cubic neighbourhood around the considered point.
- Two-dimensional bubbles detection in each plane owing to phase contrast: to locate a bubble, any of three demanding criteria (very dark, very pale, high gradient) should be fulfilled.
- A two-dimensional median morphological filter was applied in order to remove noise speckles.
- Three-dimensional averaging in a 5^3 cubic neighbourhood around the considered point. An auto-threshold by factorization [20] was then used to obtain the desired black and white (B/W) three-dimensional image.
- B/W first-neighbours three-dimensional averaging bringing back 256 grey-levels in the image, followed by a tresholding at level 127.
- For each plane, visual verifications and manual corrections.

As can be seen in figure 1, the B/W image obtained by the above procedure is generally in good agrement with the original reconstructed plane. The precision of the contour can be estimated to ± 3 voxels. Manual corrections were necessary only in regions where experimental problems happened (air bubbles producing undesired air/ice interfaces, ring artefacts, etc). They had to be done on about 15% of the processed section planes.

The three-dimensional images obtained are 600 voxel wide, which amounts to a considerable quantity of volumic data. To allow reasonable processing times for our normal and curvature algorithms, the resolution of the three-dimensional images were reduced by a factor 2 in the 3 axes. Thus, in all the three-dimensional snow images presented in this paper, one voxel corresponds to 9.82 μm.

4. Preliminary results and discussion

The model was first tested on geometrical shapes of small size, then applied to snow data and compared to the real isothermal metamorphism experiment presented in the previous part.

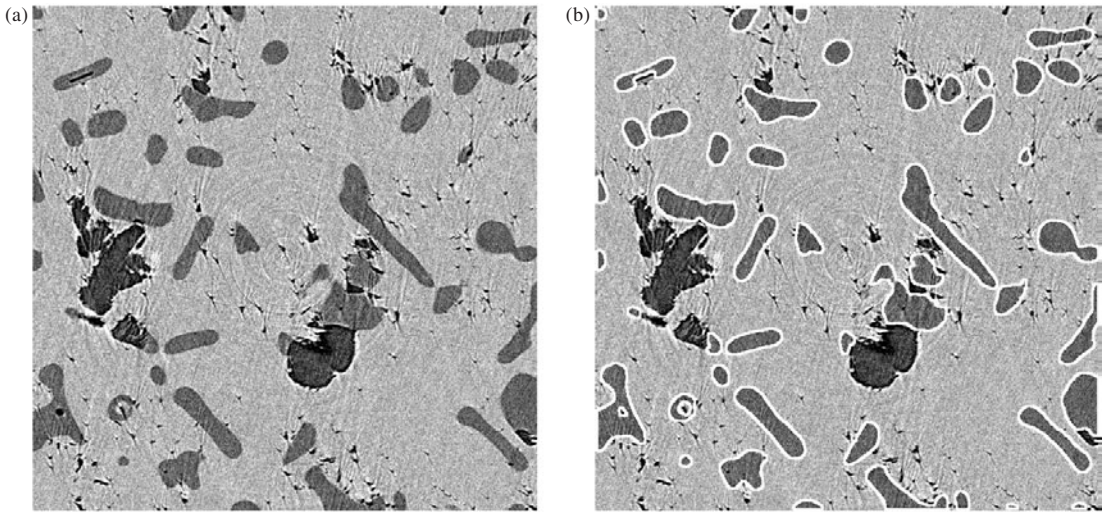

Figure 1. Image processing: a grey level original plane (*a*) and the same plane with the resulting contouring obtained (*b*), without manual corrections. The precision of the contour was estimated to ±3 voxels.

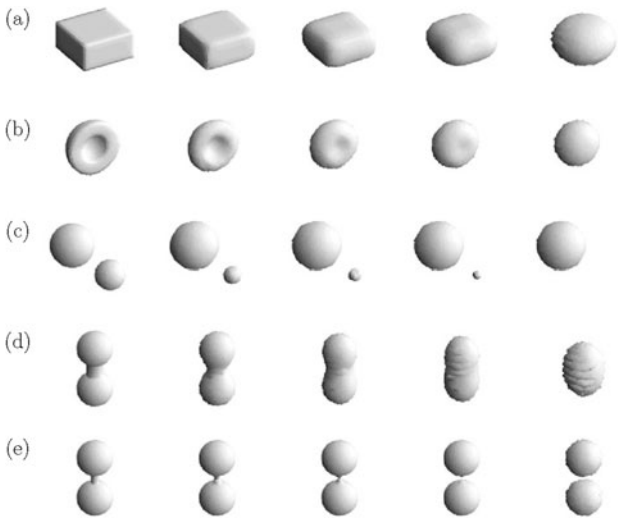

Figure 2. Metamorphism model applied on simulated data. Image edge: 64 voxels.

4.1. Validation on simulated data

The qualitative soundness of the model can be assessed by testing the well-known effects of isothermal metamorphism: edge smoothing and growth on concavities can be respectively observed in figures 2(*a*) and (*b*). The growth of the largest grains thanks to the smallest ones can be seen in figure 2(*c*). The problem of neck growth or removal is addressed in figures 2(*d*) and (*e*). The evolution of a neck is directly related to its initial size. Note that it is a typical three-dimensional phenomenon: in two dimensions, a neck is always growing, whatever its size is.

In most simulations some instabilities appear at long timescales (see the end of simulation 2(*d*)). This is due to the used curvature algorithm, which may not take into account the curvature discrepancy on small neighbourhoods. A new curvature algorithm is now in progress to solve this problem.

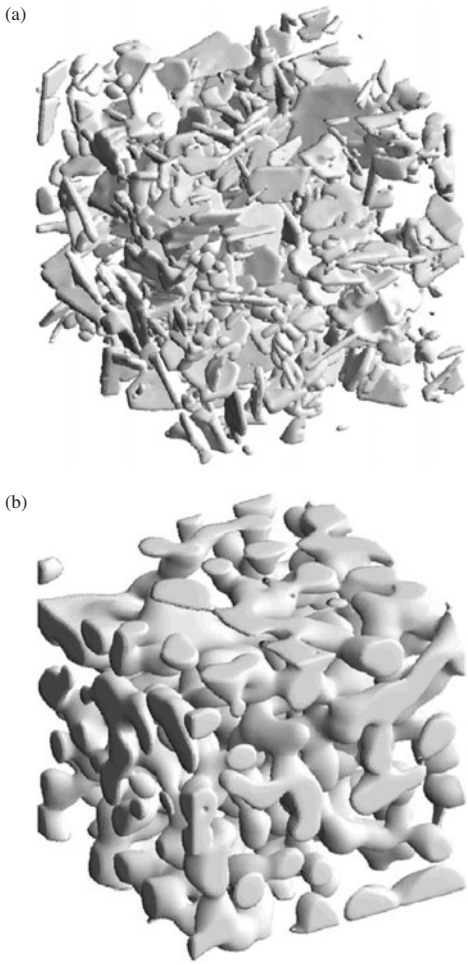

Figure 3. First (*a*) and last (*b*) stages of the isothermal experiment: grains are clearly growing and rounding during the metamorphism. Image edges are 256 voxel (∼2.5 mm) wide.

4.2. Validation on real data

In figure 4(*a*) are presented some stages given by the metamorphism model when applied on a capped column which

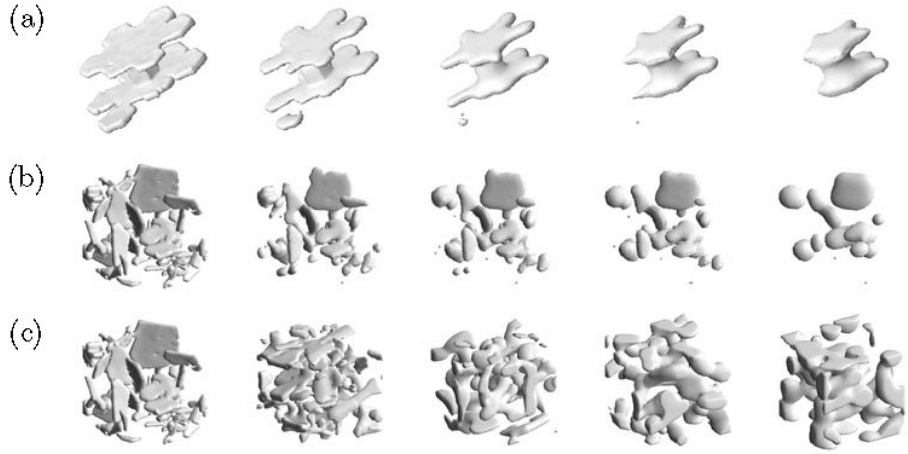

Figure 4. Metamorphism on real data: simulations on a capped column (*a*) taken in a fresh snow image (image edge: 150 voxels). Simulation (*b*) was obtained by applying the model to a subvolume of the first experimental image 3(*a*). The simulation is compared to experimental samples at the same resolution (*c*) (image edge: 128 voxels).

was extracted from a fresh snow tomographic image. Such an evolution seems very realistic, except for small remaining particles which are disappearing too slowly. As explained above, the used curvature algorithm is unable to process correctly very small neighbourhoods. As the number of such points is very small, we assume it does not disturb the general evolution of the snow particle.

In figures 3 and 4(*c*) are presented some stages of the isothermal metamorphism experiment. These figures can be compared to figure 4(*b*) where the model was applied on an extract of the first experimental image 3(*a*).

As explained in section 2.2, experimental and numerical times only differ by an undetermined constant. In the range of time considered for the experimental data, both the mean curvature and specific surface area seem to follow a logarithmic law (see figure 5). By plotting the mean curvature and specific surface area evolutions of the simulation in the same logarithmic graphics, one can observe the global soundness of the model: simulated data can be lineary fitted and have a slope error inferior to 15% of the experimental slope for the two quantities. Note that simulations where applied on subsamples of the original images: the representative volume is not reached in this case. This explains the vertical shift between simulated and real data.

To go deeper into validations, other images of the experimental metamorphism will be processed and simulations will be applied on representative volumes. Note that the real metamorphism, due to packing effects, differs from the simulated one in two significiants points: the preservation of the connectivity and the mass conservation. In the real snowpack, when a grain is disconnecting from the others, it falls on the other ones. This phenomenon is preserving the connectivity while resulting in a densification of the snow microstructure. To improve the current model, it will be necessary to simulate such gravity effects. With such an improvement, it will be possible to obtain a valuable relationship between numerical and real times. It will then be possible to discuss the soundness of the chosen evaporation–condensation mechanism.

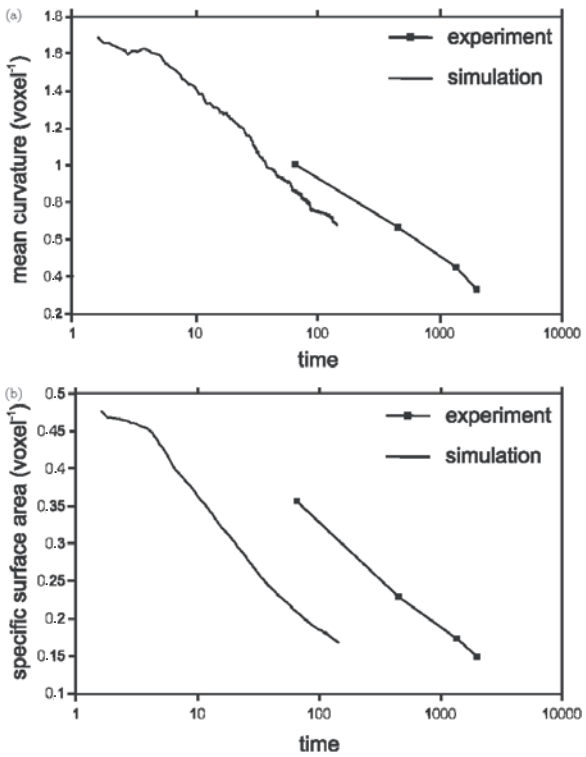

Figure 5. Mean curvature (*a*) and specific surface area (*b*) evolutions during real and simulated metamorphisms. Time is expressed in hour for real metamorphism and in numerical time (arbitrary) for simulated evolution. To allow comparison between real and simulated metamorphisms, the graphics are in logarithmic scale: the first points of each curve, where the logarithm is not defined ($t = 0$), were omitted.

5. Conclusion

A simple three-dimensional model of curvature-driven sintering has been presented together with an experiment monitoring the isothermal metamorphism of natural snow in three dimensions. This model assumes that the local mean curvature of the solid phase is the main driving force

of such transformations. Presently, some basic features of the isothermal metamorphism are already simulated on small numerical samples. The next step will be to account for grain packing (by gravity) and to speed up our curvature algorithm. By simulating a realistic sintering on 600^3 voxel images that describe a few hundred grains, we expect to check conclusively our assumption that curvature governs real isothermal metamorphism. We also expect to assess in three dimensions the importance of grain boundary effects on a real case of snow metamorphism, by comparing simulated and real concave regions. This may provide some guidelines for chosing further improvements to be implemented in models of snow microstructure.

References

[1] Colbeck S C *et al* 1990 *The International Classification for Seasonal Snow on the Ground* (Wallingford, Oxon: International Commission on Snow and Ice of the International Association of Scientific Hydrology)
[2] Colbeck S C 1998 *J. Appl. Phys.* **84** 4585–9
[3] Colbeck S C 2001 *J. Appl. Phys.* **89** 4612–8
[4] Adams E E *et al* 2001 *J. Appl. Phys.* **90** 5782–5
[5] Bullard J W 1997 *Mater. Sci. Eng.* A **238** 128–39
[6] Bullard J W 1997 *J. Appl. Phys.* **81** 159–68
[7] Brzoska J B *et al* 1999 *Eur. Phys. J. AP.* **7** 45–57
[8] Flin F *et al* 2001 *Image Anal. Stereol.* **20** 187–91
[9] Brzoska J B *et al* 2001 *Proc. 8th ECS and Image Analysis (Bordeaux, France)* Supplement 1 (Ljubljana: International Society for Stereology, ISBN 961-90933-0-5)
[10] Yanagida H *et al* 1996 *The Chemistry of Ceramics* (Chichester, England: Wiley) p 155
[11] Kingery W D 1960 *J. Appl. Phys.* **31** 833–8
[12] Kuroiwa D 1961 *Tellus* **13** 252–9
[13] Kuczynski G C 1949 *J. Metals* **1** 169–78
[14] Bannister M J 1968 *J. Am. Ceram. Soc.* **51** 548–53
[15] Hobbs P V 1974 *Ice Physics* (London: Oxford University Press) p 402
[16] Bernache-Assolant D *et al* 1993 *Chimie-physique du frittage* (Paris: Hermes) p 195
[17] Carter W C *et al* 1995 *Acta Metall. Mater.* **43** 4309
[18] Coléou C *et al* 2001 *Ann. Glaciol.* **32** 75–81
[19] Brzoska J B *et al* 1999 *ESRF Newsletter* **32** 22–3
[20] Coster M and Chermant J L 1989 *Précis d'analyse d'images* (Paris: Presses du CNRS) p 391